Journal of
Synchrotron Radiation

ISSN 0909-0495

Received 21 August 2009
Accepted 13 March 2010

In vivo high-resolution synchrotron radiation imaging of collagen-induced arthritis in a rodent model

Chang-Hyuk Choi,[a] Hong-Tae Kim,[b] Jung-Yoon Choe,[c] Seong-Kyu Kim,[c] Gi-Whan Choi,[d] SangHoon Jheon[e] and Jong-Ki Kim[f]*

[a]Department of Orthopedic Surgery, School of Medicine, Catholic University of Taegu, Taegu, Republic of Korea, [b]Department of Anatomy, School of Medicine, Catholic University of Taegu, Taegu, Republic of Korea, [c]Department of Internal Medicine, School of Medicine, Catholic University of Taegu, Taegu, Republic of Korea, [d]Department of Neurosurgery, School of Medicine, Catholic University of Taegu, Taegu, Republic of Korea, [e]Department of Thoracic Surgery, Seoul National University, Seoul, Republic of Korea, and [f]Department of Biomedical Engineering, School of Medicine, Catholic University of Taegu, Taegu, Republic of Korea. E-mail: jkkim@cu.ac.kr

In vivo microstructures of the affected feet of collagen-induced arthritic (CIA) mice were examined using a high-resolution synchrotron radiation (SR) X-ray refraction technique with a polychromatic beam issued from a bending magnet. The CIA models were obtained from six-week-old DBA/1J mice that were immunized with bovine type II collagen and grouped as grades 0–3 according to a clinical scoring for the severity of arthritis. An X-ray shadow of a specimen was converted into a visual image on the surface of a $CdWO_4$ scintillator that was magnified using a microscopic objective lens before being captured with a digital charge-coupled-device camera. Various changes in the joint microstructure, including cartilage destruction, periosteal born formation, articular bone thinning and erosion, marrow invasion by pannus progression, and widening joint space, were clearly identified at each level of arthritis severity with an equivalent pixel size of 2.7 μm. These high-resolution features of destruction in the CIA models have not previously been available from any other conventional imaging modalities except histological light microscopy. However, thickening of the synovial membrane was not resolved in composite images by the SR refraction imaging method. In conclusion, *in vivo* SR X-ray microscopic imaging may have potential as a diagnostic tool in small animals that does not require a histochemical preparation stage in examining microstructural changes in joints affected with arthritis. The findings from the SR images are comparable with standard histopathology findings.

Keywords: synchrotron radiation imaging; high-resolution phase-contrast radiography; collagen-induced arthritis (CIA) model; microstructure of joint damage; rheumatoid arthritis.

1. Introduction

Rheumatoid arthritis (RA) is the most common inflammatory joint disorder, affecting about 0.5% of adults. It is a chronic disease involving bone and joint destruction (Smith & Haynes, 2002). Much of the knowledge that has been acquired for determining new RA treatments is based on studies using experimental arthritis models. The collagen-induced arthritis (CIA) model is a very useful experimental tool for understanding the pathogenesis and therapeutic challenges of RA since it presents a destructive polyarthritis that has many clinical and radiological similarities to rheumatoid arthritis (Trentham *et al.*, 1977). Therefore, the CIA model has been used to examine the degree of synovial inflammation, periarticular change and bony structural damage, such as bony erosion, using various imaging methods (Carpenter *et al.*, 1994; Barck *et al.*, 2004; Beckmann *et al.*, 1998; Clavel *et al.*, 2008).

The evaluation of potential therapies requires techniques that quantify the severity of disease in experimental animals. Joint inflammation can be visually observed, but there are no standard methods for quantifying the degree of bone destruction in this modality. Although radiography is the gold standard for the quantification of joint destruction, it does not allow for assessing damage in soft tissues like cartilage. Radiographic criteria of RA is mostly attributed to bone erosions (Ando *et al.*, 2006; Goldring, 2002). However, the

histopathological features of RA are characterized by diverse pathological changes in the cartilage, bone and surrounding soft tissues of the joint that have been well established through histological analysis of the CIA mice model (Beckmann *et al.*, 1998; Ando *et al.*, 2006; Barck *et al.*, 2004; Larsson *et al.*, 2004; Clavel *et al.*, 2008). It is clinically important to understand these multiform pathological features in order to develop either new imaging modalities to detect changes at early stages of RA or new treatment to stop the evolution of the illness.

Histological examination is an accurate method of assessing the severity of RA lesions in humans and animals; however, histological examination requires biopsy in the patient, which is an invasive procedure. In order to carry out histological analysis in animal models of RA the animal needs to be sacrificed. This allows for evaluation of the disease at only one point in the illness evolution and prevents follow-up throughout the rest of the disease course. Although magnetic resonance imaging (MRI) may be an attractive method in the RA diagnosis, poor results have been found in some studies that attempt to demonstrate a correlation between MRI and histopathological observations (Ostergaard *et al.*, 1997, 1998; Hunter & Conaghan, 2006). Recently, the high beam coherence determined by the small X-ray source size at a third-generation SR facility has permitted the development of new imaging techniques like the 'phase-contrast' technique, which allows images of biological samples to be recorded showing superior contrast than that obtainable using conventional absorption-based X-ray imaging (Wilkins *et al.*, 1996).

This biomedical imaging method has produced high-resolution images of the microstructures of various tissues, including breast, lung and brain tumor (Bravin *et al.*, 2007; Jheon *et al.*, 2006; Pfeiffer *et al.*, 2007). Therefore, in experimental models of RA, the synchrotron radiation (SR) phase-contrast imaging method, combined with a high-resolution CCD detector, can be useful in assessing longitudinal and translational outcomes in CIA lesions *in vivo*.

In our present work, we examine the *in vivo* microstructures of affected feet joints in CIA mice using a SR phase-contrast imaging technique.

2. Materials and methods

2.1. Preparation of CIA model and immunization

Fourteen DBA/1J mice (six weeks of age; Jackson Laboratories, Bar Harbor, ME, USA) including two normal mice were used for these studies. This study protocol was approved by the ethics committee of the Catholic University Hospital of Taegu. The experimental animals were housed in a controlled environment and provided with standard rodent food and water. Bovine type II collagen (CII) (Chondrex, Redmond, WA, USA) was dissolved in 0.05 *M* acetic acid at a concentration of 2 mg ml^{-1} by stirring overnight at 277 K. The dissolved CII was then frozen at 203 K until needed. Freund's complete adjuvant (CFA) was prepared by adding *Mycobacterium tuberculosis* H37Ra at a concentration of 4 mg ml^{-1}. Before the injection, CII was emulsified with an equal volume of CFA. The CIA was induced as follows: 100 µl of the emulsion (containing 100 µg of CII) was injected intradermally at the base of the tail. After three weeks a second injection of CII in CFA was administered. After the second immunization the degree of joint inflammation was observed every other day. The severity of arthritis in each paw was assessed using a four-point clinical scoring system from 0 to 3 with 0 indicating no sign of inflammation, 1 for slight swelling and redness of the paw with the involvement of less than two joints, 2 for pronounced edema and involvement of more than two joints, and 3 for severe arthritis of the entire paw and digits with joint rigidity and ankylosis (Butler *et al.*, 1999). Two investigators (CHC and JYC) independently assessed the degree of arthritis for each mouse. Mice were grouped according to severity assessment. Two or three mice were assigned to each group.

2.2. Histological assessment of the paw joints after SR imaging

Normal control and grade 3 mice were sacrificed after SR imaging in order to assess corresponding structures in the histological sections. The removed forefoot was fixed in 10% neutral buffered formalin, decalcified in 10% EDTA and embedded in paraffin. The prepared tissue blocks of the mouse paw were then sectioned at a 10 µm thickness. The sections were stained with hematoxylin and eosin and observed by LM (light microscopy).

2.3. Phase-contrast SR imaging

The SR imaging studies were performed at the 1B2/microprobe beamline of the Pohang Light Source (PLS) in Korea. The PLS is designed to provide SR with continuous wavelengths down to 10 nm at 2.5 GeV. The experimental set-up is similar to that presented by Jheon *et al.* (2006) and Kim *et al.* (2008), and is schematically shown in Fig. 1.

Mice were anesthetized by injecting 10 ml kg^{-1} body weight of ketamine. They were imaged live attached to an acrylic plate in a supine position, thus facing the horizontal beam. The sample was positioned 25 m away from a bending-magnet source. In order to allow for mesh scanning of the sample, it

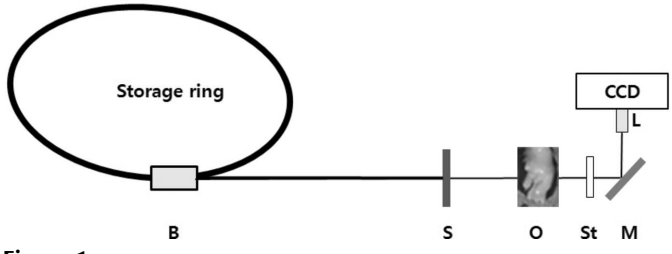

Figure 1
Schematic drawing of the experimental set-up. The polychromatic beam issued from the bending-magnet device (B) was reduced to a beam size to match the scintillator after passing through the slit (S). The X-rays irradiated the object (O) that was positioned 25 m away from the source. Visual images on the surface of the $CdWO_4$ scintillator (St) placed at a distance of 5 cm from the object were reflected at 90° by a gold-coated mirror (M) and were magnified by a microscope objective lens (×10) (L). Finally, the images reached the CCD camera (Megaplus II ES 2001).

was mounted onto a motorized XY stage and scanned. An aluminium filter (1.0 mm) was placed in the beam. Under these conditions polychromatic synchrotron X-rays were used in an energy range of 7–14 keV with a calculated dose rate between 1.6 and 3 Gy s^{-1}. The exposure time was taken between 0.5 and 1 s for scanning a view. The total dose per view was varied between 0.8 and 3 Gy.

The X-ray shadow of the specimen was converted into a visual signal on the surface of a thin (100 µm) scintillation crystal ($CdWO_4$), which was placed 5 cm away from the specimen to take advantage of the increase in phase contrast. The visual image was magnified using a ×10 microscope objective and captured using a digital CCD camera (Megaplus II ES 2001).

The fields of view of these images were determined by the size of the CCD chip and the optical magnification. For a 2.54 cm CCD camera with a ×10 microscope objective, the field of view was 1.18 mm × 0.89 mm because the CCD camera has an active area of 11.8 mm × 8.9 mm with 1600 × 1200 pixels. Therefore, each pixel corresponded to approximately 0.74 µm × 0.74 µm. The spatial resolution of our image was about 1.48 µm after a 4:1 binning process.

3. Results and discussions

3.1. Comparison of SR imaging with histology in normal feet joints

Normal joint structures visible in SR images were compared with histological slices. The results showed that the microstructures including cartilage, subchondral bone and surrounding soft tissue structures in the normal feet joints could be clearly identified in the synchrotron images and had good correlation with the histological findings (Fig. 2). Phase-contrast SR high-resolution radiography allowed us to identify the amount of articular cartilage covering a subchondral bone. In addition, each chondrocyte lacuna with a diameter of 10–30 µm was identified as a small hole. SR images exhibited well defined carpal bones, metatarsal heads and styloid processes of radial bone in normal joints that were comparable with that of conventional histological examination by light microscopy. Structural information in a slice direction was overlaid on a present propagation-based phase-contrast SR image. A composite radiographic image made of images of tissue thickening will provide more structural information than will a single histological section, as shown by comparing Figs. 2(*b*) and 2(*c*). On the other hand, such an overlaid picture may make it difficult to resolve fine structural features like synovial membranes, owing to overlapping and partial volume effects in the slice direction.

3.2. SR imaging of different severity grades of CIA

The high-resolution X-ray images of the CIA model grouped according to the severity of arthritis showed aggravated changes of joint structures and bony structures as arthritis grade increased, as shown in Fig. 3. In SR images of front limb joints and bones in higher-grade CIA mice, we observed destructive changes including loss of subchondral bone and articular cartilage, irregularities of the joint surface, and decreased radio-opacity.

Thinning and erosion of cortical and carpal bones, styloid processes of the radius, and metacarpal head loss were visualized more conspicuously in higher grades, as shown in the expanded view images of each part of the paw (Figs. 4–6).

Morphological alterations in the joint and bone of an SR image were compared with the histological images as demonstrated in Figs. 4(*B*) and 5(*A*). Destructive changes of articular structures including loss of articular cartilage (Figs. 4–6), irregularities in joint surfaces, widening of joint spaces (Fig. 6) and marrow invasions (Fig. 4*B*) were identified in the SR images. An increase of joint space that may be associated with the growth of the synovium and complete infiltration of inflammatory cells was delineated more conspicuously in the high-resolution X-ray images than in the MRI. There was decreased radio-opacity in the joint space of the grade 3 group

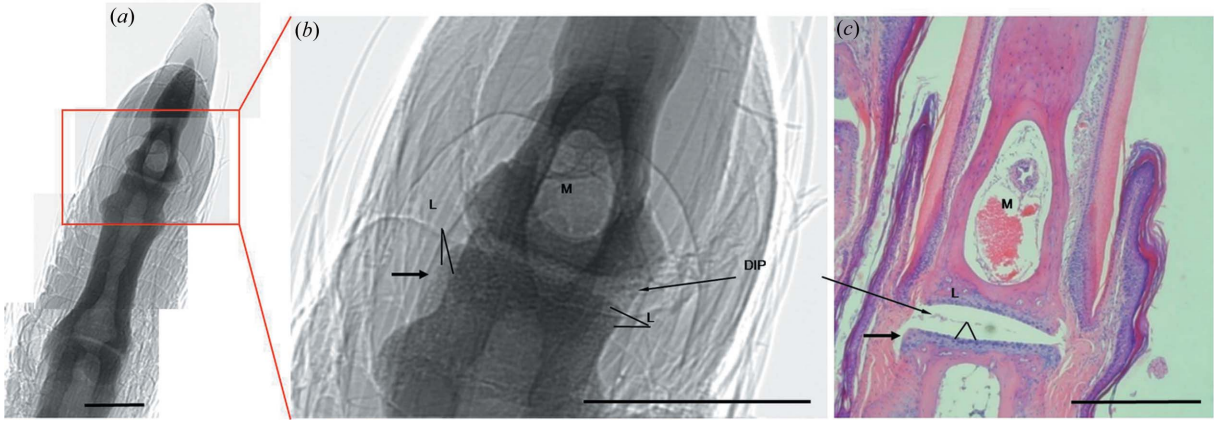

Figure 2
Phase-contrast SR high-resolution radiography images (*a*, *b*) and a histological image (*c*) of the fourth digit of the normal frontal limb. (*a*) Overlaying X-ray SR image of the whole length of the digit clearly shows joints, the alignment of phalanges and the status of the surrounding soft tissue. (*b*) Single SR image of a 1.18 mm × 0.89 mm field of view allows identification of articular cartilage (arrow), chondrocytes lacunae (L), subchondral bone and bone marrow space (M) of the distal interphalangeal joint (DIP) in detail. Scale bar = 500 µm.

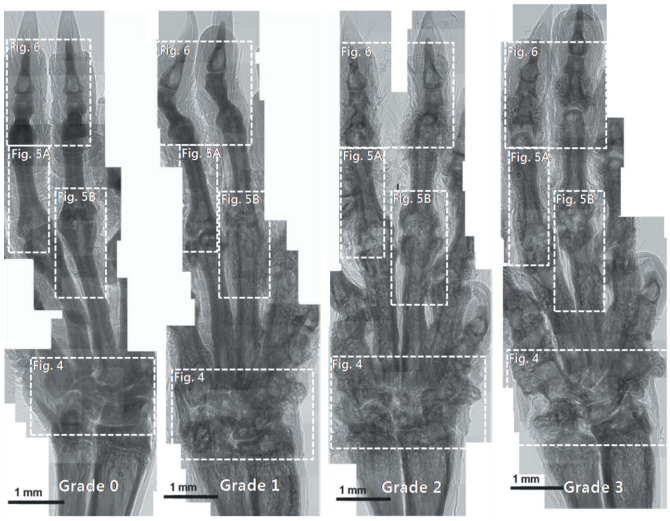

Figure 3
Comparison of phase-contrast SR micrographic images of front limbs of the CIA mice after intradermal injection of type II collagen according to severity grade. Expanded views of the boxed areas are presented in Figs. 4–6. Scale bars = 1 mm.

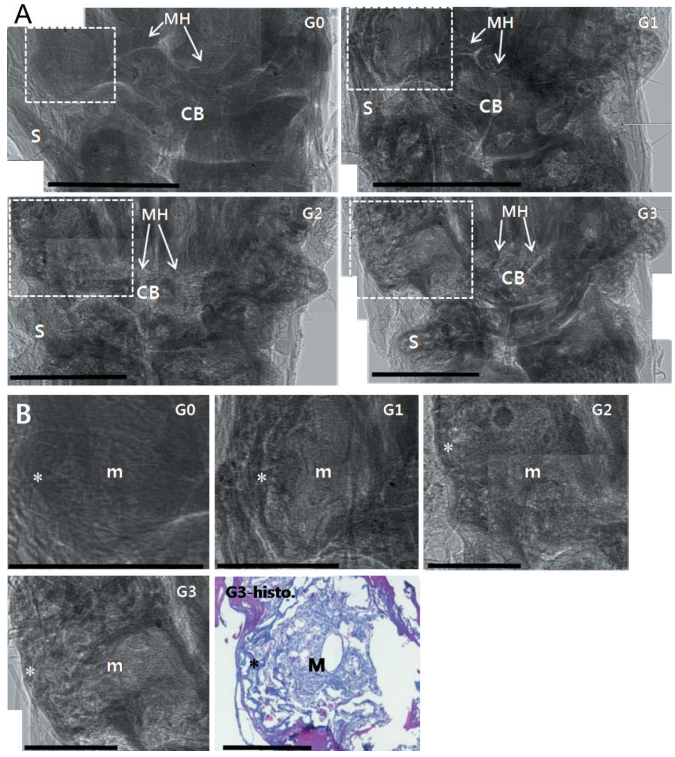

Figure 4
Comparison of SR images of carpal bones (panel *A*) and fifth metacarpal bones (panel *B*) of the CIA mice according to severity grade. The typical findings of CIA, destructive changes in cartilage and bones (CB, MH, S and *) and marrow invasion of pannus tissue (m), can be seen in the SR and histological images (G3-histo). CB: carpal bones; m: marrow cavity; MH: metacarpal bone head; S: styloid process; *: bone erosion. Scale bars = 1 mm (panel *A*) and 500 µm (panel *B*).

when compared with lower severity grades. This contrast may be associated with growth of the synovium and filling of inflammatory cells into the joint space where synovial fluid is normally present. We observed detailed loss of subchondral bone, decreased radio-opacity owing to porosity, cortical bone thinning, and erosion in SR images that were also seen in the histologic images (Figs. 4*B* and Fig. 5*A*).

Small radio-opaque fragments around thinned cortical bone were observed in the body of the phalanx in a severely diseased paw in both SR and histological images of the CIA grade 3 mice. These were confirmed as bony trabecules that had been produced from new periosteal bone formation (Figs. 5 and 6). We found that subchondral bone thinning occurred in grade 1 CIA mice, while bone was later missing in grade 3 mice (Figs. 5 and 6). Decreased radio-opacity of the marrow cavity of the fifth digit was observed and is shown in Fig. 4*B*. This may have been caused by the invasion of pannus tissue into the marrow which increased the severity of the arthritis.

The pathological findings that were identified in the SR images of each clinical grade are summarized below and are compared with the grade criteria of other imaging modalities in Table 1. Similar patterns of destruction were observed in the SR images of other imaging modalities of clinical scoring-based grades 2 and 3. However, structural damage appeared more extensive in the grade 3 group.

Grade 0. Fig. 4 shows well defined carpal bones, metatarsal heads and styloid processes of the radial bone. No typical pathological findings of CIA were observed in SR images on any part of the paw.

Grade 1. The cortical bone of the proximal phalanx, the subchondral bone of the metacarpophalangeal joint of the third digit, and the articular structure of the distal interphalangeal joint were still intact. However, destructive changes of the joint and bone, including irregularity of the joint surfaces between carpal bones, cortical bone erosion and thinning, periosteal new bone formation, and subchondral bone thinning had already begun.

Grade 2. Severe destructive changes in joints and bones were observed in almost all parts of the paw. In Fig. 4 it was difficult to define carpal bones, metacarpal heads, and styloid processes owing to the extensive destruction. Cortical bone thinning and erosion that are typical of CIA appeared in most of the phalanges and metacarpal bones. Destructive changes of articular structures including loss of articular cartilage, irregularity in joint surface, and marrow invasion of pannus tissue could be clearly identified in all joints including distal interphalangeal joints.

Grade 3. The destructive changes in bones and joints were similar to the findings of grade 2, but more extensive damage occurred over entire parts of the paw. Extensive destruction included pannus progression, bony trabecules from periosteal new bone formation, and widening of the joint space, as shown in Figs. 5 and 6.

Conventional radiographic scorings were assessed mainly by the degree of bone erosion found in the images (Devauchelle *et al.*, 2004). SR imaging findings included not only bone destruction but damage in cartilage and surrounding tissue. This is quite advantageous compared with ultrasound imaging

Table 1
Description of scoring damage in bone and joint structures of the CIA model from histology, radiographic criteria and SR imaging.

CIA grade	Grade 0	Grade 1	Grade 2	Grade 3
Histology†	No inflammatory cells in joint cavity	A few inflammatory cells	Partly filled with inflammatory cells	Totally filled with inflammatory cells
	Healthy synovium	Mild thickening of synovial membrane	Substantial thickening	Hyperplastic synovial membrane
	Normal cartilage	Minor destruction of cartilage surface	Cartilage loss, pannus formation	Cartilage absent, pannus progress
Radiographic criteria‡	No bone erosion	Mild bone erosion (shape maintained)	Severe erosion (disordered)	Ankle, subtalar, metatarsal head missing
SR imaging findings	Extent of articular cartilage, lacuna of chondrocyte (10–30 μm)	Irregularity of joint surfaces carpal bones	Loss of cartilage, marrow invasion, pannus formation	Narrow joint space, marrow invasion
	Well defined carpal bones, metatarsal head	Cortical bone erosion, periosteal new bone formation, subchondral bone thinning started	Cortical bone thinning, erosion, subchondral bone erosion	Bony trabecules formation, subchondral bone loss

† Clavel *et al.* (2008). ‡ Ando *et al.* (2006).

where destruction of the joint cannot always be detected (Szkudlarek *et al.*, 2004; Clavel *et al.*, 2008). Furthermore, this high-resolution imaging modality produced comparable findings with those of the LM investigation with regard to reflecting the degree of damage and micro-architectural changes to the joints. Observations in this study demonstrated that high-resolution SR X-ray refraction imaging can identify early inflammatory changes in the affected joint of a CIA model. In CIA, the only current way to evaluate arthritis within the paw joint is through histological analysis, which requires the animal to be sacrificed. This method of analysis only allows for the examination of a given mouse at one point

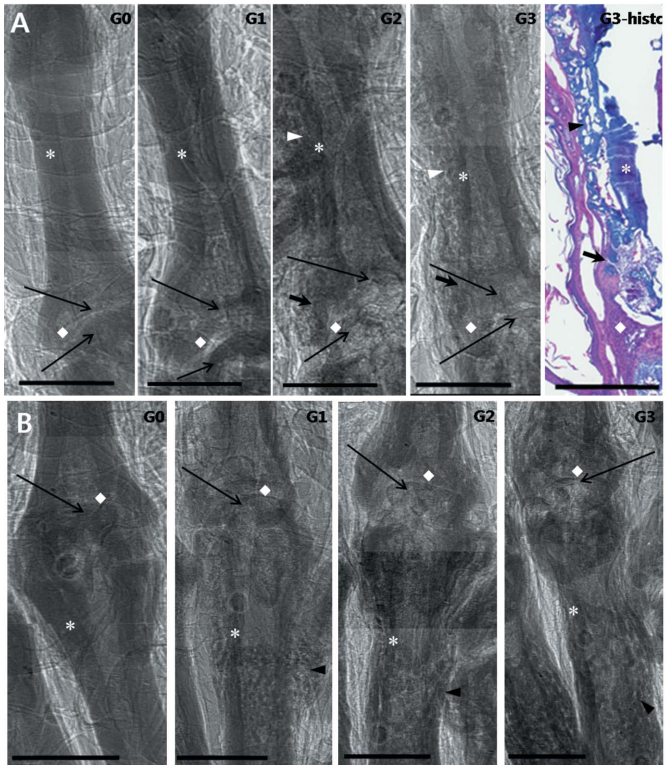

Figure 5
Comparison of SR images and a histological image (G3-histo) in MCP joints of the fourth (panel *A*) and third digits (panel *B*). The pathological features of CIA, bony and articular structures including cortical bone thinning (*) and erosion (thick arrow), periosteal bone formation (arrowhead), subchondral bone thinning and disappearance (thin arrow) and destruction of normal articular structure (diamond), could be identified in as much detail in the SR images as in the histological image. MCP: metacarpophalangeal. Scale bar = 500 μm.

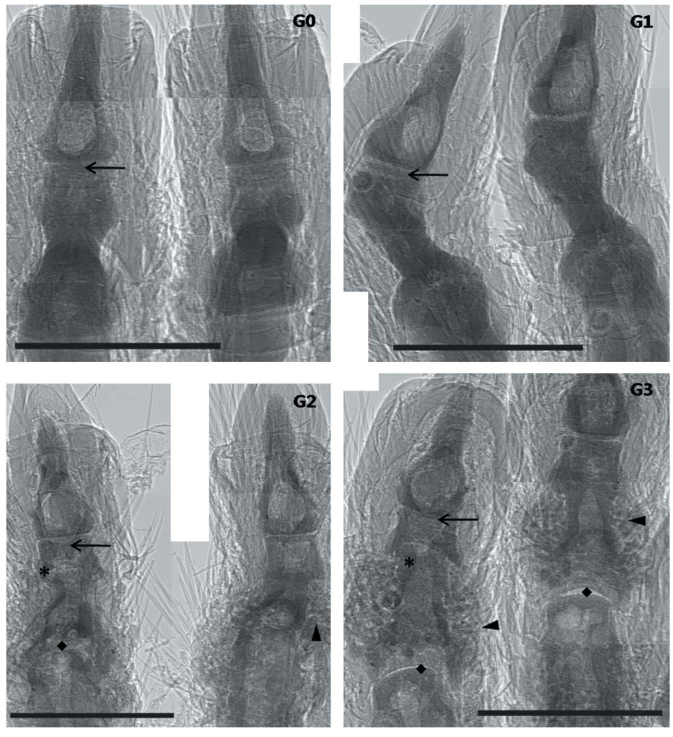

Figure 6
SR images of middle and distal interphalangeal joints of the third and fourth digits. The pathological features of CIA, bony and articular structures including cortical bone erosion (*), periosteal bone formation (arrowhead), subchondral bone thinning (thin arrow) and destruction of normal articular structure (diamond), could be identified. Scale bar = 500 μm.

in time. In this study, SR imaging allows us to evaluate arthritis in the paws of many animals for the entire duration of the course of arthritis. Therefore it is anticipated that this SR radiographic technique might play a potential role as a follow-up tool for disease activity or treatment response in RA.

3.3. Limitations of the present SR refraction imaging study in the CIA model

Thickening of the synovial membrane was not directly visualized in this SR refraction imaging study, although a phase-contrast image was acquired with high resolution of 2.7 μm. This may be due to the overlaying nature and low contrast from synovial membrane hyperplasia (SMH) for the propagation-based two-dimensional refraction imaging technique. Presently, SMH can be identified only by histological analysis. MRI microscopy and ultrasound imaging cannot demonstrate SMH in their CIA model studies owing to the low resolution of their modalities that is typically around 80 μm (Beckmann *et al.*, 1995; Clavel *et al.*, 2008). Imaging of SMH would be highly important because of its relevance to the early diagnosis of RA. Tomographic images with mono-energetic X-rays issued from a SR source would be suitable to resolve SMH of the CIA model, by using one of the three phase-contrast imaging techniques: interferometry, analyzer-based imaging (ABI) or grating interferometry. X-ray interferometry is the most sensitive method for detecting the small differences in refractive index of soft tissues (Momose *et al.*, 1998). ABI and grating interferometry are capable of revealing the contrast generated not only from absorption but also from refraction and extinction arising from the internal structures of the object examined (Chapman *et al.*, 1997; Pfeiffer *et al.*, 2006). These structures may provide either refraction-sensitive or diffraction-sensitive phase contrast at the tissues interfaces.

Rheumatoid arthritis is accompanied by three types of bone loss: focal articular bone erosion, juxta-articular osteopenia adjacent to inflamed joints, and systemic osteoporosis (Goldring & Gravallese, 2000). It is clear that radiographic joint destruction is strongly associated with systemic osteoporosis (Forsblad D'Elia *et al.*, 2003; Sambrook, 2000). A general decrease in the radio-opacity, owing to increasing porosity in higher-grade CIA, was observed in the front limb bones of CIA mice. This suggests that phase-contrast SR imaging can potentially diagnose juxta-articular osteopenia adjacent to inflamed joints more clearly and at an earlier stage than can conventional radiographic techniques. In this regard, mono-energetic X-ray beams should be used in SR imaging to quantitatively detect opacity changes as a measure of bone porosity or bone mineral density (BMD) without the beam-hardening effect of conventional BMD techniques. Although this was not realised in this propagation-based two-dimensional imaging experiment, recent SR micro-CT studies demonstrated quantitative analysis of bone mineral density and micro-architecture *in vivo* in a rodent model (Bayat *et al.*, 2005; Matsumoto *et al.*, 2006). These estimations showed the feasibility of this methodology by measuring fractional bone volume from high-resolution three-dimensional imaging of the trabecular bone architecture and calculating BMD based on linear attenuation coefficient values.

3.4. Radiation dose limitation of polychromatic SR imaging

The radiation doses delivered in this study were quite high compared with those of conventional radiography. This may constitute a real limitation to the use of polychromatic SR in non-invasive *in vivo* imaging. The main reason for using polychromatic SR was to obtain a sufficient X-ray flux penetrating the sample thickness for imaging with a detector system. A 7 keV monochromatic X-ray beam, the highest X-ray energy with maximum flux, was available from a monochromator at the current 1B2 beamline of Pohang Accelerator Laboratory (PAL), but this energy is not able to penetrate a sample thicker than 2 mm. Although delivered doses could be reduced by using an automatic fast shutter to stop the beam between two exposures or a detector system with higher detective quantum efficiency (Bravin *et al.*, 2003), they will remain very high because of the ultra-high resolution applied for this examination.

Currently PAL is undergoing an upgrade project to increase injector energy up to 3 GeV, and to prepare a multipole-wiggler-type insertion device that will provide an enhanced X-ray flux over a large energy range (20–60 keV) for biomedical imaging application. When this project is completed, the radiation dose necessary for producing monochromatic SR X-ray images in the 20–60 keV energy range would be similar to that necessary to produce images of the same samples with a detector combined with an anti-scatter grid as used in clinical imaging (Burattini *et al.*, 1995).

4. Concluding remarks

Observations in this study demonstrated that high-resolution SR X-ray refraction imaging can identify early inflammatory changes and associated bone erosion in the affected joints of a CIA model in mice with fine pathological features that are comparable with those of histological analysis. Further developments in SR imaging may be necessary to resolve synovial membrane hyperplasia using more sophisticated phase-contrast tomographic techniques with a mono-energetic beam.

This work was supported by a grant (2009-0088454) from the National Research Foundation of Korea and a grant from Institute of Medical Science, Catholic University of Taegu.

References

Ando, W., Hashimoto, J., Nampei, A., Tsuboi, H., Tateishi, K., Ono, T., Nakamura, N., Ochi, T. & Yoshikawa, H. (2006). *J. Bone Miner. Metab.* **24**, 274–282.

Barck, K. H., Lee, W. P., Diehl, L. J., Ross, J., Gribling, P., Zhang, Y., Nquven, K., van Bruqqen, N., Hurst, S. & Carano, R. A. (2004). *Arthritis Rheum.* **50**, 3377–3386.

Bayat, S., Apostol, L., Boller, E., Brochard, T. & Peyrin, F. (2005). *Nucl. Instrum. Methods Phys. Res. A*, **548**, 247–252.

Beckmann, N., Bruttel, K., Mir, A. & Rudin, M. (1995). *Magn. Res. Imaging*, **13**, 1013–1017.
Beckmann, N., Bruttel, K., Schuurman, H. & Mir, A. (1998). *J. Magn. Res.* **131**, 8–16.
Bravin, A., Fiedler, S., Coan, P., Labiche, J.-C., Ponchut, C., Peterzol, A. & Thomlinson, W. (2003). *Nucl. Instrum. Methods Phys. Res. A*, **510**, 35–40.
Bravin, A., Keyriläinen, J., Fernández, M., Fiedler, S., Nemoz, C., Karjalainen-Lindsberg, M.-L., Tenhunen, M., Virkkunen, P., Leidenius, M., von Smitten, K., Sipil, P. & Suortti, P. (2007). *Phys. Med. Biol.* **52**, 2197–2211.
Burattini, E., Cossu, E., Maggio, C. D., Gambaccini, M., Indovina, P. L., Marziani, M., Pocek, M., Simeoni, S. & Simonetti, G. (1995). *Radiology*, **195**, 239–244.
Butler, D. M., Malfait, A. M., Maini, R. N., Brennan, F. M. & Feldmann, M. (1999). *Eur. J. Immunol.* **29**, 2205–2212.
Carpenter, T. A., Everett, J. R., Hall, L. D., Harper, G. P., Hodgson, R. J., James, M. F. & Watson, P. J. (1994). *Skelet. Radiol.* **23**, 429–CCCC437.
Chapman, D., Thomlinson, W., Johnston, R. E., Washburn, D., Pisano, E., Gműr, N., Zhong, Z., Menk, R., Arfelli, F. & Sayers, D. (1997). *Phys. Med. Biol.* **42**, 2015–2025.
Clavel, G., Marchiol-Fournigault, C., Renault, G., Boissier, M.-C., Fradelizi, D. & Bessis, N. (2008). *Ann. Rheum. Dis.* **67**, 1765–1772.
Devauchelle, P. V., Saraux, A., Berthelot, J. M., Alapetite, S., Jousse, S., Chales, G., Thorel, J. B., Hoang, S., Nouy-Troll, I., Martin, A., Chiocchia, G., Youinou, P. & LeGoff, P. (2004). *J. Rheumatol.* **31**, 66–70.
Forsblad D'Elia, H., Larsen, A. & Waltbrand, E. (2003). *Ann. Rheum. Dis.* **62**, 617–623.
Goldring, S. R. (2002). *Curr. Opin. Rheumatol.* **14**, 406–410.
Goldring, S. R. & Gravallese, E. M. (2000). *Arthritis Res.* **2**, 33–37.
Hunter, D. J. & Conaghan, P. G. (2006). *Curr. Opin. Rheumatol.* **18**, 157–162.
Jheon, S. H., Youn, H.-S., Kim, H.-T., Choi, G.-H. & Kim, J.-K. (2006). *Microsc. Res. Tech.* **69**, 656–659.
Kim, B.-I., Kim, K.-H., Youn, H.-S., Jheon, S., Kim, J.-K. & Kim, H.-T. (2008). *Microsc. Res. Tech.* **71**, 443–447.
Larsson, E., Erlandsson Harris, H., Larsson, A., Månsson, B., Saxne, T. & Klareskog, L. (2004). *Rheumatology*, **43**, 428–434.
Matsumoto, T., Yoshino, M., Asano, T., Uesugi, K., Todoh, M. & Tanaka, M. (2006). *J. Appl. Physiol.* **100**, 274–280.
Momose, A., Takeda, T., Itai, Y., Yoneyama, A. & Hirano, K. (1998). *Medical Applications of Synchrotron Radiation*, edited by M. Ando and C. Uyama, pp. 63–71. Tokyo: Springer-Verlag.
Ostergaard, M., Stoltenberg, M., Lovgreen-Nielsen, P., Volck, B., Jensen, C. H. & Lorenzen, I. (1997). *Arthritis Rheum.* **40**, 1856–1867.
Ostergaard, M., Stoltenberg, M., Lovgreen-Nielsen, P., Volck, B., Sonne-Holm, S. & Lorenzen, I. (1998). *Magn. Reson. Imaging*, **16**, 743–754.
Pfeiffer, F., Bunk, O., David, C., Bech, M., Le Duc, G., Bravin, A. & Cloetens, P. (2007). *Phys. Med. Biol.* **52**, 6923–6930.
Pfeiffer, F., Weitkamp, T., Bunk, O. & David, C. (2006). *Nat. Phys.* **2**, 258–261.
Sambrook, P. (2000). *J. Rheumatol.* **27**, 2541–2542.
Smith, J. B. & Haynes, M. K. (2002). *Ann. Intern. Med.* **136**, 908–922.
Szkudlarek, M., Narvestad, E., Klarlund, M., Court-Payen, M., Thomsen, H. S. & Ostergaard, M. (2004). *Arthritis Rheum.* **50**, 2103–2112.
Trentham, D. E., Townes, A. S. & Kang, A. H. (1977). *J. Exp. Med.* **146**, 857–868.
Wilkins, S. W., Gureyev, T. E., Gao, D., Pogany, A. & Stevenson, A. W. (1996). *Nature (London)*, **384**, 335–338.